ARTICLE

doi:10.1038/nature13976

β-catenin mediates stress resilience through Dicer1/microRNA regulation

Caroline Dias[1]*, Jian Feng[1]*, Haosheng Sun[1], Ning yi Shao[1], Michelle S. Mazei-Robison[1]†, Diane Damez-Werno[1], Kimberly Scobie[1], Rosemary Bagot[1], Benoit LaBonté[1], Efrain Ribeiro[1], XiaoChuan Liu[1], Pamela Kennedy[1]†, Vincent Vialou[1]†, Deveroux Ferguson[1]†, Catherine Peña[1], Erin S. Calipari[1], Ja Wook Koo[1], Ezekiell Mouzon[1], Subroto Ghose[2], Carol Tamminga[2], Rachael Neve[3], Li Shen[1] & Eric J. Nestler[1]

β-catenin is a multi-functional protein that has an important role in the mature central nervous system; its dysfunction has been implicated in several neuropsychiatric disorders, including depression. Here we show that in mice β-catenin mediates pro-resilient and anxiolytic effects in the nucleus accumbens, a key brain reward region, an effect mediated by D2-type medium spiny neurons. Using genome-wide β-catenin enrichment mapping, we identify *Dicer1*—important in small RNA (for example, microRNA) biogenesis—as a β-catenin target gene that mediates resilience. Small RNA profiling after excising β-catenin from nucleus accumbens in the context of chronic stress reveals β-catenin-dependent microRNA regulation associated with resilience. Together, these findings establish β-catenin as a critical regulator in the development of behavioural resilience, activating a network that includes Dicer1 and downstream microRNAs. We thus present a foundation for the development of novel therapeutic targets to promote stress resilience.

Despite decades of research, the molecular pathophysiology of depression remains elusive. One molecular player implicated in neuropsychiatric illnesses, including depression, is β-catenin[1–5]. In addition to having a structural role at synapses, β-catenin mediates the transcriptional output of canonical Wnt signalling[6–8]. This multi-functionality has made it difficult to untangle the mechanism through which β-catenin might contribute to pathological states. We recently demonstrated the involvement of upstream Wnt signalling in the nucleus accumbens (NAc) in mouse depression models, with impaired signalling mediating susceptibility to social stress and increased signalling mediating resilience[9]. We thus began by studying the behavioural role of β-catenin in this brain region.

β-catenin mediates resilience and anxiolytic responses

We overexpressed β-catenin in a herpes simplex virus (HSV) vector in NAc (Fig. 1a; Extended Data Fig. 1a), which increases β-catenin solely in the nuclear compartment, as measured by subcellular fractionation and immunohistochemistry (IHC), whereas global N-cadherin/β-catenin complexes were unaffected (Extended Data Fig. 1b, c). This suggests that HSV-β-catenin selectively activates the transcriptional function of the protein, without having direct effects on N-cadherin at synapses, consistent with earlier work in cultured cells[10].

We next overexpressed β-catenin in NAc during accelerated social defeat stress (ASD)[11,12]. We found that, while HSV-GFP injected control animals developed social avoidance, an indicator of depression-like behaviour, overexpression of β-catenin prevented this phenotype (Fig. 1b). Furthermore, in baseline behavioural assays, β-catenin mediated an antidepressant-like response in the forced swim test (FST) (Fig. 1c), and anxiolytic effects in the elevated plus maze (EPM) (Fig. 1d). We saw no changes in sucrose preference or cocaine conditioned place preference (data not shown), suggesting that β-catenin does not cause hedonic changes. To confirm the pro-resilient effect of β-catenin, we used a stabilized β-catenin mutant (S33Y)[13], and found identical results for wild-type β-catenin in the ASD and FST (Supplementary Notes), with no change in sucrose preference (data not shown). Finally, cell-type-specific overexpression of β-catenin in D2- but not D1-type medium spiny neurons (MSNs) in NAc (Fig. 1e, Extended Data Fig. 2a) induced a pro-resilient phenotype.

We also investigated the consequences of blocking β-catenin signalling in NAc with two approaches: excising β-catenin from NAc of conditional floxed mice (Extended Data Fig. 2b) and overexpressing a behaviourally validated dominant negative β-catenin mutant (Extended Data Fig. 2c)[14]. Both manipulations promoted susceptibility to stress in mice subjected to a sub-threshold defeat procedure (Fig 1f, g). Excising β-catenin from NAc caused no change in social interaction or locomotion in control animals, demonstrating a specific association with stress (Extended Data Fig. 3a–c). These results establish a critical role for β-catenin signalling in NAc in behavioural resilience.

To explore the endogenous activity of β-catenin in depression, we examined its transcriptional activity in post-mortem NAc of depressed humans. Axin2, a universal readout of activated canonical β-catenin signalling, was robustly suppressed in NAc of depressed humans (Fig. 2a, Supplementary Table 1, Extended Data Fig. 4a). In contrast, total N-cadherin and β-catenin messenger RNA levels were unchanged, pointing specifically to β-catenin nuclear function alterations in depression. There was also suppression of Tcf3 and Tcf4 (T cell transcription factors 3 and 4) levels in depressed patients (Fig. 2a); these are two of several transcription factors through which β-catenin acts. Together, these data demonstrate downregulation of the transcriptional output of β-catenin in NAc in human depression.

We next investigated *Axin2* mRNA levels in mouse NAc 48 h after chronic social defeat stress (CSDS). We found no difference between

[1]Fishberg Department of Neuroscience and Friedman Brain Institute, Icahn School of Medicine at Mount Sinai, New York, New York 10029, USA. [2]Department of Psychiatry, University of Texas Southwestern, Dallas, Texas 75390, USA. [3]Department of Brain and Cognitive Sciences, Massachusetts Institute of Technology, Cambridge, Massachusetts 02139, USA. †Present addresses: Department of Physiology, Michigan State University, East Lansing, Michigan 48824, USA (M.S.M.-R.); Department of Psychology, UCLA College of Life Sciences, Los Angeles, California 90095, USA (P.K.); Institut National de la Santé et de la Recherche Médicale (INSERM) U1130; CNRS UMR8246; UPMC UM18, Neuroscience Paris Seine, 75005 Paris, France (V.V.); Department of Basic Medical Sciences, The University of Arizona College of Medicine-Phoenix, Arizona 85004, USA (D.F.).
*These authors contributed equally to this work.

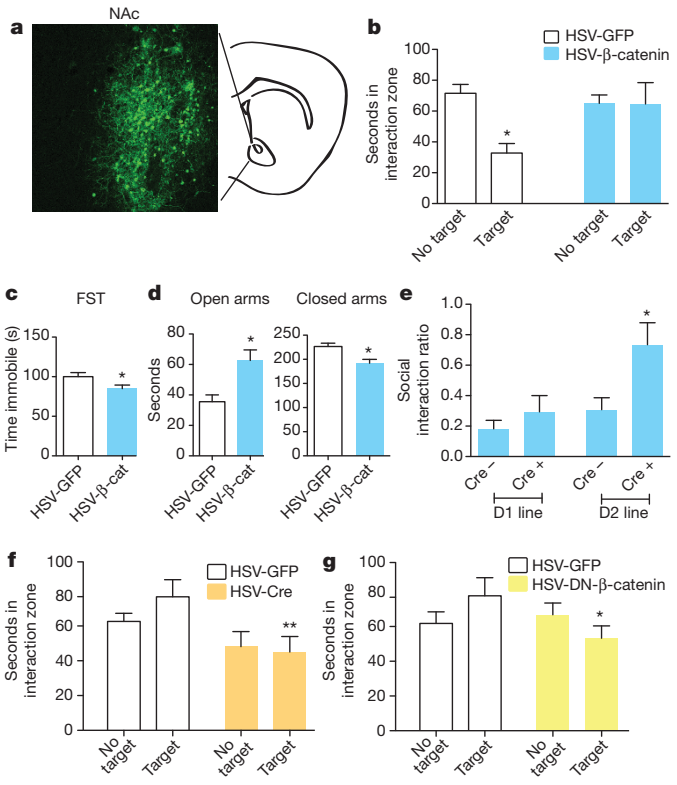

Figure 1 | β-catenin in NAc mediates pro-resilient, antidepressant, and anxiolytic responses. **a**, IHC illustrating viral transgene expression mediated by HSV-β-catenin with coronal cartoon of NAc highlighted. **b**, Pro-resilient effect of HSV-β-catenin on social interaction after ASD (*$P < 0.05$, two way ANOVA, $n = 8$ GFP, $n = 10$ β-catenin). **c**, Antidepressant-like effect of β-catenin in the forced swim test (*$P < 0.05$, two-tailed t-test, $n = 6$ GFP, $n = 7$ β-catenin). **d**, Anxiolytic-like effect of β-catenin in the elevated plus maze (closed arms: *$P < 0.01$, open arms: *$P < 0.01$, two-tailed t-test, $n = 6$ GFP, $n = 7$ β-catenin). **e**, Cell-type-specific overexpression of β-catenin in ASD (D2 Cre^- versus Cre^+: *$P < 0.05$, two-tailed t-test, $n = 13$ D2 Cre^-, $n = 8$ D2 Cre^+). **f**, Effect of knocking down β-catenin in a sub-threshold defeat procedure (**$P < 0.01$, two-way ANOVA, effect of virus only when target present, $n = 6$ GFP, $n = 5$ Cre). **g**, Effect of dominant negative β-catenin in sub-threshold defeat (*$P < 0.05$, two-way ANOVA, interaction effect, $n = 5$ GFP, $n = 4$ dominant negative). Data presented as mean and s.e.m. and are representative of at least two experiments. See Methods and Supplementary Table 9 for detailed statistics.

susceptible and resilient animals (Fig. 2b). However, resilient animals displayed increased Tcf3 and Tcf4, indicating that resilience may be associated with upregulation of β-catenin signalling (Fig. 2b). To probe this, we examined the levels of phospho-Ser 675 β-catenin, a form with enhanced transcriptional activity, as well as total β-catenin at this time point. We found upregulation in resilient versus susceptible animals of phospho-Ser 675 β-catenin but not total β-catenin (Extended Data Fig. 4b). At 10 days after CSDS, we found elevated levels of Axin2 in resilient mice only ($P < 0.05$, Supplementary Notes).

Cell-type-specific action of β-catenin in resilience

Given the small magnitude of change observed above, we questioned whether the cell-type-specific behavioural effects in Fig. 1e corresponded to differential regulation of β-catenin signalling in D2 versus D1 MSNs. Using fluorescence-assisted cell sorting-isolated NAc neurons from D2-GFP mice (whereby the D2 neurons are labelled with green fluorescent protein, GFP), we found robust induction of Axin2 expression in $D2^+$ neurons of resilient mice, and significantly reduced Axin2 levels in susceptible versus resilient mice, 48 h post CSDS, effects not seen in $D2^-$ cells (Fig. 2c). Furthermore, Axin2 IHC with D1- or D2-GFP transgenic mice subjected to CSDS revealed downregulation of β-catenin transcriptional activity in D2 versus D1 MSNs in susceptible mice (Fig. 2d). In sum, upregulation of β-catenin signalling occurs in D2 MSNs in resilient mice, with downregulation seen in susceptible animals.

Because glutamatergic neurotransmission regulates β-catenin transcriptional activity and stress susceptibility[15,16], we tested whether medial prefrontal cortex (PFC) or hippocampus, two important glutamatergic inputs to NAc, control β-catenin signalling in NAc. Using previously validated constructs and stimulation protocols[17,18], we found that optogenetic stimulation of glutamatergic PFC terminals robustly suppressed β-catenin activity in NAc as indicated by decreased Axin2, Tcf3, and Tcf4, whereas stimulation of hippocampus terminals had no effect (Fig. 2e, f). Repeated burst firing of dopamine afferents from the ventral tegmental area (VTA) also had no effect (Extended Data Fig. 5). Thus, PFC to NAc stimulation specifically elicited a molecular 'signature' of susceptibility, indicating that activation of this circuit could mediate the maladaptive suppression of β-catenin activity in NAc.

Genome-wide mapping of β-catenin after social defeat

We next conducted β-catenin chromatin immunoprecipitation followed by deep sequencing (ChIP-seq) on NAc of control, susceptible, and resilient mice after CSDS. We first validated our β-catenin ChIP protocol by examining an LEF/TCF consensus sequence in the promoter of a known β-catenin target gene, *CaMKIV* (also known as *Camk4*). We found enrichment of β-catenin at the LEF/TCF site, but not a distant site, in NAc of resilient mice only (Fig. 3a). Through ChIP-seq[19,20] we then examined global β-catenin enrichment after CSDS, and found major differences in peak numbers (Fig. 3b, Supplementary Data 1). Control and resilient conditions were associated with 10–15-fold higher absolute peak numbers compared to susceptible conditions, suggesting profound global alterations in β-catenin activity, consistent with our biochemical data (Fig. 2). Enrichment of β-catenin in resilient animals (Fig. 3b) only occurred at transcriptionally active sites, as indicated by high basal binding of two transcriptional activation marks H3K4me3 and H4K16ac (Fig. 3c, Extended Data Fig. 6). However, we did not observe global changes in these two histone marks after CSDS (Extended Data Figs 7, 8), suggesting that β-catenin may be recruited to active, open regions of chromatin through the presence of other, direct DNA-binding transcription factors.

Using Ingenuity pathway analysis, we demonstrated a predicted β-catenin network to be upregulated in NAc of resilient versus susceptible mice (Extended Data Fig. 9), a prediction specific to β-catenin. Concomitantly, there were nearly twice as many increases as decreases in β-catenin binding in resilient versus control mice at promoter regions. In contrast, susceptible versus control animals displayed equivalent numbers of upregulated and downregulated β-catenin binding events (Fig. 3d). These results support our hypothesis that resilience is associated with genome-wide enrichment of β-catenin. Examining the distribution of β-catenin peaks across the genome (Fig. 3e) revealed similar results: redistribution of β-catenin binding towards promoters and gene bodies in resilience, and redistribution away from promoters/gene bodies and towards gene deserts in susceptibility.

To validate the β-catenin ChIP-seq data, we conducted quantitative ChIP (qChIP) on independent biological samples at genes that showed significant peaks in resilience or upregulation in resilient versus susceptible animals, thus confirming significant β-catenin enrichment at several promoters (Fig. 3f). As further validation, we examined mRNA levels of genes found in our ChIP-seq list that coincided either with *in silico* lists of predicted or known β-catenin targets[21,22] (Supplementary Table 2) or with the H3K4me3 and H4K16ac ChIP-seq data sets (Supplementary Data 2). We found robust upregulation of many of these genes in NAc of resilient mice (Fig. 3g).

Regulation of Dicer1 and microRNA by β-catenin

One gene validated by qChIP and quantitative PCR (qPCR) was *Dicer1*, a critical component of microRNA (miRNA) biogenesis[23]. Thus, selective enrichment of β-catenin binding at *Dicer1* in resilient mice (Fig. 4a),

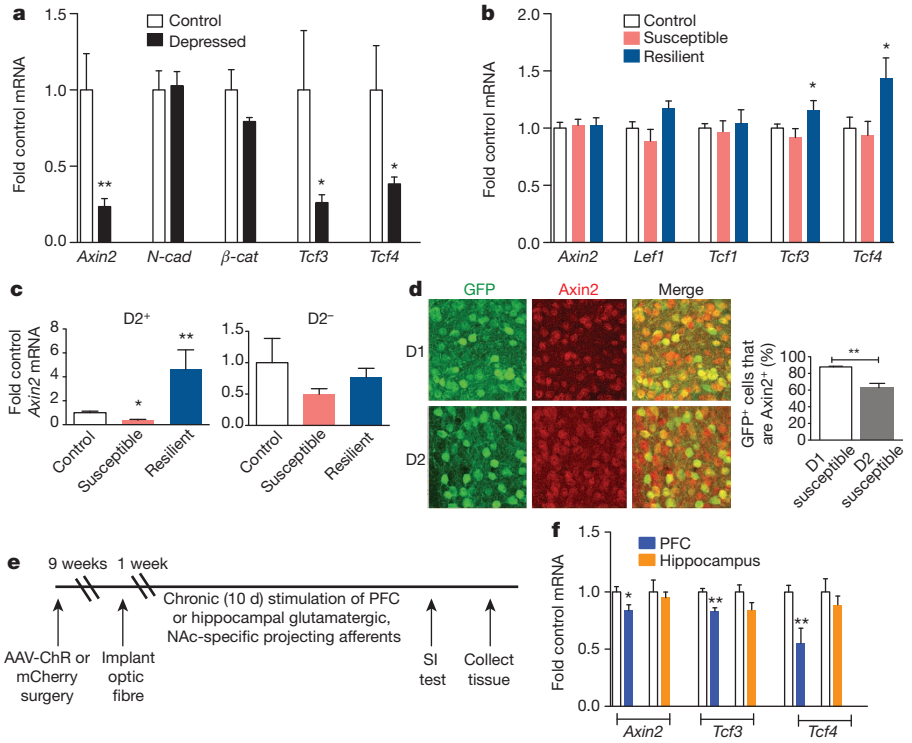

Figure 2 | Regulation of β-catenin signalling in human depression and mouse CSDS. **a**, mRNA from human NAc (*Axin2*: $^{**}P < 0.01$; *Tcf3*: $^{*}P < 0.05$; *Tcf4*: $^{*}P < 0.05$, two-tailed *t*-test, $n = 6$ control, $n = 10$ depressed). **b**, mRNA from mouse control, susceptible, and resilient NAc 48 h post CSDS (*Tcf3*: $^{*}P < 0.05$; *Tcf4*: $^{*}P < 0.05$, one-way ANOVA, $n = 16$ control, $n = 12$ susceptible, $n = 9$ resilient). **c**, *Axin2* is upregulated in $D2^{+}$ MSNs only in resilience (*Axin2* $D2^{+}$:$^{**}P < 0.01$, control versus resilient $P < 0.05$, $^{*}P < 0.01$ susceptible versus resilient, $n = 4$ control, $n = 5$ susceptible, $n = 3$ resilient; *Axin2* $D2^{-}$: not significant, $P > 0.05$, $n = 3$ control, $n = 5$ susceptible, $n = 3$ resilient, one-way ANOVA). **d**, Percentage of cells positive for Axin2 plus GFP in D1- or D2-GFP susceptible mice after CSDS ($^{**}P < 0.01$, two-tailed *t*-test, $n = 3$ per group). **e**, Optogenetic stimulation protocol. **f**, mRNA expression in NAc after repeated stimulation from PFC or hippocampus in ChR2 versus mCherry (*Axin2*: $^{*}P < 0.05$, $n = 6$ mCherry, $n = 5$ ChR; *Tcf3*: $^{**}P < 0.01$, $n = 6$ mCherry; $n = 4$ ChR; *Tcf4*: $^{**}P < 0.01$, $n = 6$ mCherry, $n = 4$ ChR, two-tailed *t*-test). Human data are from one experiment, all other data are representative of at least two experiments. All data presented as mean and s.e.m.

and subsequent validation of this effect (Fig. 3f, g), indicated that *Dicer1* represents a robust target of β-catenin in NAc. To study the behavioural effects of Dicer1, we knocked it down locally in NAc (Extended Data Fig. 10), and conducted sub-threshold defeat. Control animals injected with HSV-GFP displayed normal social interaction; however, animals with Dicer1 knockdown demonstrated social avoidance (Fig. 4b), which mimicked the effects of blocking β-catenin signalling (Fig. 1). Importantly, we can rule out confounding effects of long-term Dicer1 loss on neuronal viability[24], because our experimental paradigm was limited to two weeks.

To assess whether the behavioural effect of Dicer1 was related to β-catenin signalling, we first expressed HSV-Cre or HSV-GFP in NAc of floxed *Dicer1* mice and found no difference in social interaction under baseline, non-stressed conditions (Fig. 4c). We then injected all mice with HSV-β-catenin in NAc and subjected them to ASD. β-catenin overexpression blocked the development of social avoidance in mice

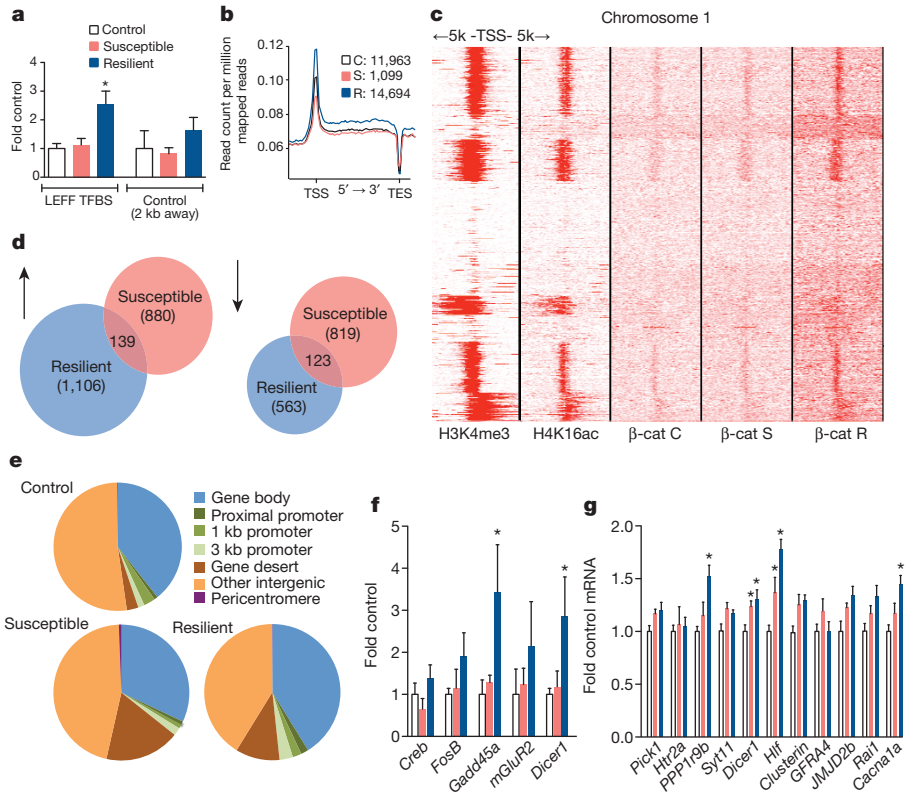

Figure 3 | β-catenin ChIP-seq in NAc 48 h post CSDS. **a**, qChIP validation of β-catenin ChIP ($^{*}P < 0.05$, one-way ANOVA, post-hoc test control versus resilient and susceptible versus resilient at LEFF transcription factor binding site (TFBS) of a CaMKIV gene, $n = 4$ per group). **b**, Plot of β-catenin binding across genic regions. TSS, transcription start site; TES, transcription end site. Individual peak numbers per condition indicated in inset. **c**, Heat map showing β-catenin binding 5 kb up- and downstream of TSSs on chromosome 1 in control (C), susceptible (S), and resilient (R) NAc; binding profiles of H3K4me3 and H4K16ac under basal conditions are also shown. **d**, Number of increased (up arrow) versus decreased (down arrow) β-catenin binding sites at promoters in resilient versus control or susceptible versus control conditions. **e**, Genome-wide distribution of β-catenin binding. **f**, qChIP validation of ChIP-seq (*Gadd45a*: $^{*}P < 0.05$, one-way ANOVA; *Dicer1*: $^{*}P < 0.05$, one-way ANOVA, $n = 4$ control, susceptible, $n = 3$ resilient). **g**, mRNA validation of β-catenin ChIP-seq (*Dicer1*: $^{*}P < 0.01$, one-way ANOVA, $n = 13$ control, $n = 11$ susceptible, $n = 7$ resilient). Data presented as mean and s.e.m. and are representative of at least two experiments. Colour-coding in **f** and **g** as in **a**.

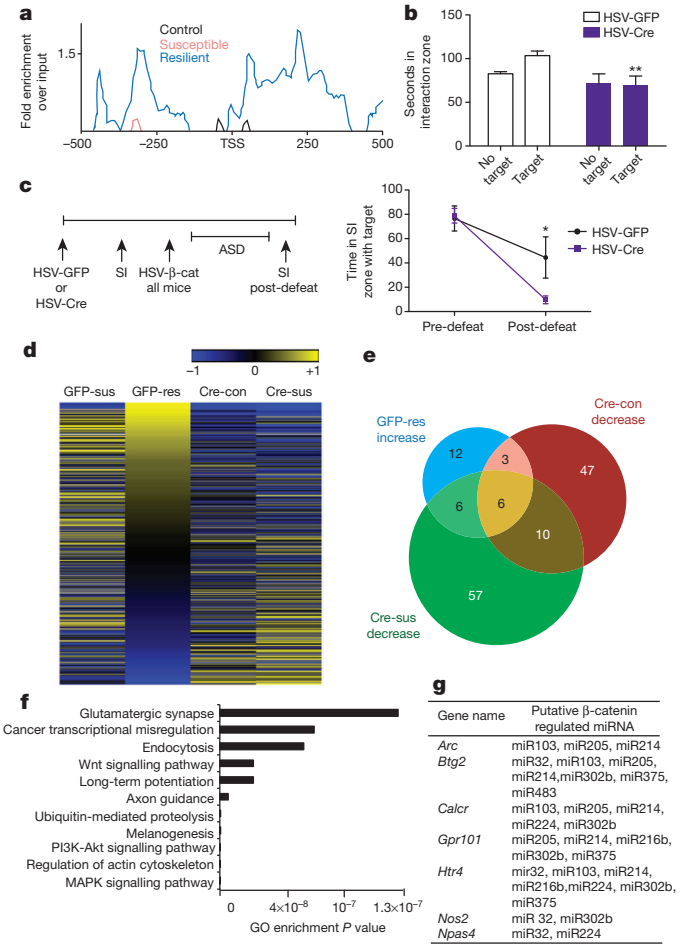

Figure 4 | Dicer1 bridges β-catenin and miRNA regulation in CSDS. **a**, β-catenin ChIP-seq enrichment around the Dicer1 TSS. **b**, Effect of NAc Dicer1 knockdown (HSV-Cre) in sub-threshold defeat with HSV-GFP as control (**$P < 0.01$, effect of virus, two-way ANOVA, $n = 7$ Cre, $n = 8$ GFP). **c**, Left, schematic of floxed Dicer1 deletion followed by β-catenin rescue; right, social interaction (SI) before and after ASD with HSV-β-catenin (*$P < 0.05$, interaction effect, matching two-way ANOVA, $n = 7$ per group). **d**, Heat map of CSDS-regulated miRNA expression changes with (Cre) or without (GFP) β-catenin knockdown. Log_2-fold changes of all altered miRNAs among all groups are shown. **e**, Venn diagram showing increased miRNAs in GFP-resilient mice (GFP-res) overlap with decreased miRNAs in β-catenin knockout in non-stressed (Cre-con) or susceptible (Cre-sus) animals. **f**, Top 11 most enriched gene ontology terms of target genes of overlapping miRNAs in panel **e**. **g**, Predicted targets of β-catenin-dependent miRNAs display downregulation by mRNA-seq in resilient mice after CSDS. Data presented as mean and s.e.m. and are representative of at least two experiments.

expressing normal Dicer1 levels, but not in mice with NAc Dicer1 knockdown (Fig. 4c). This indicates that at least part of the pro-resilient effect of β-catenin is mediated through Dicer1.

Finally, these data prompted us to examine the global miRNA profile in NAc in response to CSDS and study its dependence on β-catenin. We injected an adeno-associated virus (AAV) vector expressing GFP or Cre in NAc of floxed β-catenin mice, subjected them to CSDS or control conditions, and performed small RNA sequencing (Supplementary Table 3). We first compared each group—GFP susceptible (GFP-sus), GFP resilient (GFP-res), Cre control (Cre-con), and Cre susceptible (Cre -sus)—to the 'GFP-con' condition. We could not study the Cre resilient condition, because virtually no mice are resilient upon β-catenin knockout from NAc. We found downregulation of numerous miRNAs, including many that were upregulated in resilience, when β-catenin was knocked out from control animals (Cre-con, Fig. 4d, Supplementary Table 4). Interestingly, a smaller subset of miRNAs was upregulated following β-catenin knockout, which may represent miRNAs that are regulated by repressive factors under β-catenin control. We identified 66 miRNAs that were significantly downregulated in NAc after β-catenin deletion (Cre-con, Fig. 4e). We also identified downregulated miRNAs ($n = 79$) in the Cre-sus condition, many of which were decreased in Cre-con, further substantiating our hypothesis that pro-adaptive miRNA responses are lost in the absence of β-catenin, enhancing susceptibility to stress (Fig. 4e). miRNAs that overlapped between any two groups (up in GFP-res, but down in Cre-con or Cre-sus), presumably represent the most biologically important β-catenin- and stress-regulated miRNAs (Fig. 4e, Supplementary Table 5). This subset controls several meaningful gene categories (Fig. 4f), including Wnt and glutamatergic signalling. Finally, to identify potential miRNA targets, we overlapped predicted targets of these β-catenin-regulated miRNAs (Supplementary Table 5) with mRNA-seq data from NAc after CSDS. We thus found several interesting, novel genes to be significantly repressed in resilience (Fig. 4g).

We also examined other small RNAs for regulation by CSDS. Piwi-interacting RNAs (piRNAs), small RNAs widely studied in germ line cells, were detected recently in brain and found to play a functional role in spine morphology and synaptic plasticity[25,26]. 163 piRNAs were detectable in our data set with read counts in at least one condition, supporting the notion of piRNA expression in brain (Supplementary Table 6). Although the majority of them were expressed at low levels, approximately 20 piRNAs appear to be regulated by CSDS (Supplementary Table 7). Examining additional small RNA categories that might be regulated by Dicer1 revealed several differentially expressed candidates (Supplementary Table 8), laying the groundwork for future investigation.

Discussion

The present study demonstrates that β-catenin in D2 MSNs activates a network in NAc that mediates behavioural resilience, whereas deficits in this pathway contribute to depression-related pathology. PFC inputs to NAc appear to be particularly important in controlling this β-catenin regulation. D2 MSNs, which comprise the indirect or 'no-go' pathway[27–30], may be more important for mediating flexible behavioural choices in aversive contexts compared to reward-motivated behaviour[31–33]. We thus posit that enhanced β-catenin signalling in NAc D2 MSNs of resilient mice permits increased behavioural flexibility, which allows them, despite having the same experience as susceptible mice, to overcome generalizing avoidance of all mice, a process independent of hedonic responses. This has parallels in humans: resilient individuals are more successful at managing stress and recovering from it[34].

Our β-catenin ChIP-seq approach provides a valuable resource for mining the molecular targets that drive resilience. One validated target is Dicer1, which establishes a novel connection between β-catenin signalling and miRNAs in brain. Among the regulated miRNAs are those that feedback and regulate β-catenin signalling[35]. The cell type-specific role of β-catenin, and the inherent complexity of stress susceptibility versus resilience, which involves many additional regulatory steps beyond Dicer1, presumably explains the relatively small number of β-catenin-dependent miRNAs observed in this study. miRNAs provide a crucial layer of post-transcriptional gene regulation in neural development, plasticity, and in an increasing number of brain disorders[36–38]. The present study, by identifying specific miRNAs associated with stress susceptibility or resilience, offers a template for future studies to induce resilience in inherently more susceptible individuals.

Online Content Methods, along with any additional Extended Data display items and Source Data, are available in the online version of the paper; references unique to these sections appear only in the online paper.

Received 12 August 2013; accepted 20 October 2014.
Published online 12 November 2014.

1. Madsen, T. M., Newton, S. S., Eaton, M. E., Russell, D. S. & Duman, R. S. Chronic electroconvulsive seizure up-regulates β-catenin expression in rat hippocampus: role in adult neurogenesis. *Biol. Psychiatry* **54,** 1006–1014 (2003).

2. Beaulieu, J.-M. *et al.* Lithium antagonizes dopamine-dependent behaviors mediated by an AKT/glycogen synthase kinase 3 signaling cascade. *Proc. Natl Acad. Sci. USA* **101,** 5099–5104 (2004).
3. Gould, T. D. *et al.* Beta-catenin overexpression in the mouse brain phenocopies lithium-sensitive behaviors. *Neuropsychopharmacology* **32,** 2173–2183 (2007).
4. Li, X. & Jope, R. S. Is glycogen synthase kinase-3 a central modulator in mood regulation? *Neuropsychopharmacology* **35,** 2143–2154 (2010).
5. Brennand, K. J. *et al.* Modelling schizophrenia using human induced pluripotent stem cells. *Nature* **473,** 221–225 (2011).
6. Behrens, J., von Kries, J., Kühl, M. & Bruhn, L. Functional interaction of β-catenin with the transcription factor LEF-1. *Nature* **382,** 638–642 (1996).
7. Molenaar, M. *et al.* XTcf-3 transcription factor mediates β-catenin-induced axis formation in *Xenopus* embryos. *Cell* **86,** 391–399 (1996).
8. van de Wetering, M. *et al.* Armadillo coactivates transcription driven by the product of the *Drosophila* segment polarity gene dTCF. *Cell* **88,** 789–799 (1997).
9. Wilkinson, M. B. *et al.* A novel role of the WNT-dishevelled-GSK3β signaling cascade in the mouse nucleus accumbens in a social defeat model of depression. *J. Neurosci.* **31,** 9084–9092 (2011).
10. Sadot, E. *et al.* Regulation of S33/S37 phosphorylated β-catenin in normal and transformed cells. *J. Cell Sci.* **115,** 2771–2780 (2002).
11. Berton, O. *et al.* Essential role of BDNF in the mesolimbic dopamine pathway in social defeat stress. *Science* **311,** 864–868 (2006).
12. Krishnan, V. *et al.* Molecular adaptations underlying susceptibility and resistance to social defeat in brain reward regions. *Cell* **131,** 391–404 (2007).
13. Kolligs, F. T., Hu, G., Dang, C. V. & Fearon, E. R. Neoplastic transformation of RK3E by mutant β-catenin requires deregulation of Tcf/Lef transcription but not activation of c-*myc* expression. *Mol. Cell. Biol.* **19,** 5696–5706 (1999).
14. Wang, Z. *et al.* β-catenin promotes survival of renal epithelial cells by inhibiting Bax. *J. Am. Soc. Nephrol.* **20,** 1919–1928 (2009).
15. Rada, P. *et al.* Glutamate release in the nucleus accumbens is involved in behavioral depression during the Porsolt swim test. *Neuroscience* **119,** 557–565 (2003).
16. Abe, K. & Takeichi, M. NMDA-receptor activation induces calpain-mediated β-catenin cleavages for triggering gene expression. *Neuron* **53,** 387–397 (2007).
17. Tye, K. M. *et al.* Amygdala circuitry mediating reversible and bidirectional control of anxiety. *Nature* **471,** 358–362 (2011).
18. Britt, J. P. *et al.* Synaptic and behavioral profile of multiple glutamatergic inputs to the nucleus accumbens. *Neuron* **76,** 790–803 (2012).
19. Feng, J. *et al.* Chronic cocaine-regulated epigenomic changes in mouse nucleus accumbens. *Genome Biol.* **15,** R65 (2014).
20. Shen, L. *et al.* diffReps: detecting differential chromatin modification sites from ChIP-seq data with biological replicates. *PLoS ONE* **8,** e65598 (2013).
21. Hödar, C. *et al.* Genome-wide identification of new Wnt/β-catenin target genes in the human genome using CART method. *BMC Genomics* **11,** 348 (2010).
22. Wexler, E. M. *et al.* Genome-wide analysis of a Wnt1-regulated transcriptional network implicates neurodegenerative pathways. *Sci. Signal.* **4,** ra65 (2011).
23. Bernstein, E., Caudy, A. A., Hammond, S. M. & Hannon, G. J. Role for a bidentate ribonuclease in the initiation step of RNA interference. *Nature* **409,** 363–366 (2001).
24. Cuellar, T. L. *et al.* Dicer loss in striatal neurons produces behavioral and neuroanatomical phenotypes in the absence of neurodegeneration. *Proc. Natl Acad. Sci. USA* **105,** 5614–5619 (2008).
25. Lee, E. J. *et al.* Identification of piRNAs in the central nervous system. *RNA* **17,** 1090–1099 (2011).
26. Rajasethupathy, P. *et al.* A role for neuronal piRNAs in the epigenetic control of memory-related synaptic plasticity. *Cell* **149,** 693–707 (2012).
27. Graybiel, A. M. The basal ganglia. *Curr. Biol.* **10,** R509–R511 (2000).
28. Gerfen, C. R. The neostriatal mosaic: multiple levels of compartmental organization in the basal ganglia. *Annu. Rev. Neurosci.* **15,** 285–320 (1992).
29. Kravitz, A. V., Tye, L. D. & Kreitzer, A. C. Distinct roles for direct and indirect pathway striatal neurons in reinforcement. *Nature Neurosci.* **15,** 816–818 (2012).
30. Lobo, M. K. & Nestler, E. J. The striatal balancing act in drug addiction: distinct roles of direct and indirect pathway medium spiny neurons. *Front. Neuroanat.* **5,** 41 (2011).
31. Hikida, T., Kimura, K., Wada, N., Funabiki, K. & Nakanishi, S. Distinct roles of synaptic transmission in direct and indirect striatal pathways to reward and aversive behavior. *Neuron* **66,** 896–907 (2010).
32. Darvas, M. & Palmiter, R. Contributions of striatal dopamine signaling to the modulation of cognitive flexibility. *Biol. Psychiatry* **69,** 704–707 (2011).
33. Yawata, S., Yamaguchi, T., Danjo, T., Hikida, T. & Nakanishi, S. Pathway-specific control of reward learning and its flexibility via selective dopamine receptors in the nucleus accumbens. *Proc. Natl Acad. Sci. USA* **109,** 12764–12769 (2012).
34. Southwick, S. M. & Charney, D. S. The science of resilience: implications for the prevention and treatment of depression. *Science* **338,** 79–82 (2012).
35. Veronese, A. *et al.* Mutated β-catenin evades a microRNA-dependent regulatory loop. *Proc. Natl Acad. Sci. USA* **108,** 4840–4845 (2011).
36. Kosik, K. S. The neuronal microRNA system. *Nature Rev. Neurosci.* **7,** 911–920 (2006).
37. Im, H.-I. & Kenny, P. J. MicroRNAs in neuronal function and dysfunction. *Trends Neurosci.* **35,** 325–334 (2012).
38. Issler, O. *et al.* MicroRNA 135 is essential for chronic stress resiliency, antidepressant efficacy, and intact serotonergic activity. *Neuron* **83,** 344–360 (2014).

Supplementary Information is available in the online version of the paper.

Acknowledgements We thank O. Jabado and M. Mahajan for support and S. Borkan for providing β-catenin constructs. This work was supported by grants from the National Institute of Mental Health and the Hope for Depression Research Foundation (HDRF).

Author Contributions C.D. and J.F. conceived the project, designed research, conducted experiments, interpreted the results, and wrote the manuscript; H.S., M.S.M.-R., D.D.-W., K.S., R.B., B.L., E.R., P.K., V.V., D.F., C.P., E.C., J.K. and E.M. conducted experiments; S.G., C.T. provided reagents and tools; R.N. conducted experiments and provided reagents; N.S., X.L. performed bioinformatic analysis; L.S. performed and supervised bioinformatic analysis; E.J.N. conceived the project, designed and supervised research, interpreted the results, and wrote the manuscript. All authors discussed the results and commented on the manuscript.

Author Information All sequencing data have been deposited into the Gene Expression Omnibus with accession numbers GSE61294 and GSE61295. Reprints and permissions information is available at www.nature.com/reprints. The authors declare no competing financial interests. Readers are welcome to comment on the online version of the paper. Correspondence and requests for materials should be addressed to E.J.N. (eric.nestler@mssm.edu) or L.S. (li.shen@mssm.edu).

METHODS

Animals. For all experiments, 7–9-week-old male mice were used. Unless otherwise noted for transgenic lines, c57bl/6 mice from Jackson Laboratories were used. All mice were housed on a 12-h light/dark cycle with ad libitum access to food and water. CD1 retired breeder mice were obtained from Charles River Laboratories. The following transgenic mouse lines were used. From Jackson Laboratories: β-catenin conditional floxed mice (stock no. 004152) and Dicer1 conditional floxed mice (stock no. 006001). Additionally, D1-Cre, D2-Cre, D1-GFP, and D2-GFP male mice that were backcrossed to a c57bl/6 background were used for experiments as described in the text. For the D1-Cre/D2-Cre cell-type specific overexpression experiments, wild-type littermates were used as controls. The Mount Sinai Institutional Animal Care and Use Committee approved all animal protocols used in this study. For all experiments, extensive laboratory experience was used to estimate required sample sizes. Animals were randomly assigned to experimental groups and whenever possible, experimenters were blinded to the group. (For example, in behavioural experiments by assigning numbers to animals and in IHC experiments by hiding group designation until after quantification and analysis.)

Viral-mediated gene transfer. Stereotactic surgery was performed on mice under ketamine/xylazine anaesthesia. Vectors were infused bilaterally into NAc at a rate of 0.1 μl min^{-1} with the following coordinates: +1.6 mm anterior-posterior (A/P), +1.5 mm medial-lateral (M/L), ± 4.4 mm dorsal-ventral (D/V) from bregma. A total of 0.5 μl per side was infused except for the HSV-LS virus, in which case 0.7 μl was infused total. All vectors used were cloned into p1005 HSV or LS1L HSV. Mouse β-catenin constructs were provided by S. Borkan (Boston University). Wild-type and dominant negative constructs were used, with the dominant negative construct containing amino and carboxy-terminal truncations. Because this is a complicated mutant, we behaviourally validated it by demonstrating a failure to rescue β-catenin loss of function impairments in social interaction (Extended Data Fig. 2c). Human β-catenin S33Y construct (Addgene Plasmid no. 19286) was originally from E. Fearon (Michigan). This mutant contains an S33Y mutation that prevents phosphorylation at Ser 33 by GSK3β, thus preventing β-catenin degradation. For cell-type-specific overexpression, an HSV carrying β-catenin in a lox-stop cassette was used (Supplementary Fig. 2a) in conjunction with D1- and D2-Cre transgenic mouse lines. Viral-Cre was used for local knockdown of β-catenin or Dicer1 in conditional floxed mice.

Behaviour. 10-day chronic social defeat stress (CSDS), an accelerated 4-day defeat procedure (ASD), and a sub-threshold defeat procedure have been described previously and represent an ethologically validated model of depression[9,11,12] We used ASD over 4 days (4 days of defeat, twice a day) to coincide with periods of maximal HSV-mediated transgene expression in some experiments as described, which induces the same degree of behavioural deficits in normal mice as our standard 10-day CSDS procedure. For all defeats, social interaction was measured either 24 h or 1 week following the last defeat. For all tissue analysis, including ChIP, mice were killed 48 h after the last defeat (24 h after social interaction) of a 10 day CSDS paradigm unless otherwise specified. Elevated plus maze and forced swim tests were performed as described previously[12].

Post-mortem human tissue. Human post-mortem NAc complementary DNA was generated and analysed as before[9]. Briefly, brain tissue was obtained from the Dallas Brain Collection, where tissue is collected from the Dallas Medical Examiner's Office and UT Southwestern's Tissue Transplant Program following consent of next-of-kin. Tissue was analysed and matched for age, post-mortem interval, RNA integrity number (RIN), and pH (see Supplementary Table 1) and this same tissue set was used in previously published work[39]. Samples were subjected to a standard dissection before snap freezing in −40 °C isopentane and storage at −80 °C; further dissection of NAc was performed on frozen tissue. The UT Southwestern Institutional Review Board reviewed and approved the collection of this tissue for research use. We should note that there was no difference in expression of Axin2 between medicated and unmedicated depressed patients, although all patients were clinically depressed at their time of death (Supplementary Fig. 4a). We thus combined the medicated and unmedicated groups into one overall depressed group as presented in Fig. 2.

RNA isolation and qPCR. RNA was extracted and purified using a protocol combining TRIzol/chloroform extraction with the Qiagen RNeasy Micro kit, with a motorized mini-pestle vibrator to homogenize the tissue. After extraction, purity and concentration were measured on a NanoDrop spectrophotometer. RNA was then reverse transcribed into cDNA with the iScript DNA synthesis kit (Bio-Rad). *GAPDH* was used to normalize quantification. Primers were designed to flank exon/intron boundaries and were created using the open-source software Primer3. Real-time qPCR analysis was performed with the $\Delta\Delta C_t$ method to obtain relative fold-change of expression as compared to control samples[40]. BLAST and dissociation curve analysis was also performed to ensure specificity of primer design.

Western blotting. NAc was dissected bilaterally using 14 gauge steel circular punches. The tissue was then sonicated in radioimmunoprecipitation assay (RIPA) buffer with a desktop sonicator (10 mM Tris, pH 7.4, 150 mM NaCl, 1 mM EDTA, 0.1% SDS, 1% Triton X-100, 1% sodium deoxycholate, with protease and phosphatase inhibitors) and centrifuged. The supernatant was collected and the protein concentration was quantified using the Lowry method. Laemelli sample buffer was added to the protein lysate and equal amounts of protein were loaded onto precast SDS–PAGE gels with molecular weight ladders. Samples were transferred to activated PVDF membranes, blocked, and incubated in primary antibody overnight. Blots were washed, and then incubated with Licor secondary fluorescent antibodies. After further washing, the blots were scanned and images analysed with ImageJ software. The following antibodies were used: phospho-Ser 675 β-catenin (Cell Signaling no. 4176; Ser 675 is phosphorylated by PKA), total β-catenin (Cell Signaling no. 9562), GAPDH, β-tubulin, and total H3. All antibodies are commercially available and have been validated for use in the laboratory. Pre-incubating the tissue with calf intestinal phosphatase and demonstrating a decrease in signal was performed to validate the phospho-Ser 675 β-catenin antibody.

Optogenetics. For glutamatergic nerve terminal stimulation, mice were injected unilaterally with AAV-CAMKIIa-ChR2-mCherry or AAV-CAMKIIa-mCherry with the coordinates of: (−3.6 A/P, +3.05 M/L, −4.85 D/V) for ventral hippocampus and (+1.9 A/P, +0.5 M/L, −3.0 D/V) for PFC unilaterally. After 9 weeks of recovery to allow for expression in terminals, a second stereotactic surgery was performed to implant an optic fibre targeting the NAc shell with coordinates of (+1.4 A/P, +1.5 M/L, −4 D/V), again unilaterally, ipsilateral to virus expression. After allowing one week for recovery, the mice underwent 10 days of daily 5-min stimulation sessions outside of their home cage as described[41,42]. Stimulation parameters were either 20 Hz, 30 pulses per burst, with 10 s between bursts (hippocampus); or 30 Hz, 90 pulses per burst, 10 s between bursts (PFC) to roughly balance the relative intensity of NAc innervation from these two afferent regions. Unilateral NAc tissue was then dissected 48 h later for biochemical experiments. Constructs and stimulation parameters have been previously validated[17,18]. AAV-ChR2 was used to stimulate VTA cell bodies with a phasic protocol (20 Hz, 5 spikes per burst, 10 s between bursts) given susceptible mice exhibit increased firing rate and bursting events following defeat[12,43].

Co-immunoprecipitation (Co-IP). A co-IP kit (Roche) was used as follows. 4 punches of NAc were lysed in 300 μl of the provided lysis buffer. 10% total lysate was reserved and the rest was centrifuged and the supernatant transferred to a clean microcentrifuge tube. It was pre-cleared by incubation with protein G-agarose for 3 h on a rotator at 4 °C. The beads were centrifuged, and the supernatant was transferred to fresh tubes, where they were incubated with 5 μl of β-catenin antibody (Cell Signaling no. 9581) for one hour before 50 μl of a homogeneous protein G-agarose suspension was added and then incubated overnight at 4 °C on a rotator. The complexes were centrifuged and the supernatant was removed, the beads were washed twice with lysis buffer 1, twice with buffer 2, and once with buffer 3. Protein sample buffer was added and the samples boiled for 3 min. Complexes were then analysed as described under western blotting.

Nuclear/cytoplasmic fractionation. NAc punches were homogenized with a glass Dounce tissue grinder and loose pestle in Buffer A (1 M Tris-HCl, 1 M sucrose, 1 M DTT, protease and phosphatase inhibitors). 10% of the lysate was reserved to assay total protein levels, and the rest was centrifuged at 1,450 r.c.f. in an Eppendorf 5417c centrifuge for 10 min. The supernatants were then removed, centrifuged at 5,970 r.c.f. in the same centrifuge for 7 min, and the resulting supernatants were stocked as the cytoplasmic fraction. Buffer B (1 M Tris-HCl pH 7.5, 0.1 M EDTA, 0.1 M EGTA, 1 M sucrose, 1 M DTT, 10% NP-40, protease and phosphatase inhibitors) was added to the pellets from the first centrifugation and the samples were kept on ice for 10 min before centrifuging again at 1,450 r.c.f. in the same centrifuge for 10 min. The supernatants were discarded and Buffer C (1 M Tris-HCl, 37.5% glycerol, 5 M NaCl, 0.1 M EDTA, 0.1 M EGTA, 1 M DTT, 10% NP-40, protease and phosphatase inhibitors) was used to re-suspend the nuclear fraction. The fractions were then processed for western blotting as above or further separated into chromatin and non-chromatin nuclear fractions. Tubulin and total H3 were used as loading controls and to verify appropriate cytoplasmic and nuclear enrichment.

Immunohistochemistry (IHC). Mice were anaesthetized with chloral hydrate followed by trans-cardial perfusion of 10 ml of filtered PBS, followed by 25 ml of filtered 4% paraformaldehyde (PFA) in PBS, pH 7.4. Brains were dissected out and post-fixed overnight in PFA. They were then rinsed in PBS and placed in 30% sucrose in PBS. For the IHC in Fig. 2, once the brains sank, coronal 35-μm sections through the NAc were taken on a freezing microtome and kept in PBS with 0.01% sodium-azide. The slices were washed 3× in PBS for 10 min and then blocked for 3–4 h (3% normal goat serum, 0.3% TritPBS) in net wells. They were incubated in primary antibody overnight diluted in block (rabbit Anti-Axin2, Abcam; Mouse Anti-GFP, Life Technologies) at 4 degrees. The slices were then washed 3× in PBS, followed by a 1-h incubation in secondary antibody (Alexa-Fluor Anti-Rabbit & Anti-Mouse 680 & 800 diluted 1:1,000 in PBS). The slices were washed 4× in PBS and then mounted on charged slides and allowed to dry overnight. They were

dehydrated, coverslipped with Depex mounting medium, and sealed with clear nail polish. *Z*-stacks were taken on a Zeiss LSM 710 confocal microscope at ×64 magnification. Settings were kept identical for all images taken. The specificity of the Axin2 antibody was validated by competing the antibody with the immunizing protein. Average values of 3–5 images per mouse were used. For quantification purposes, the percent of $Axin2^{+}GFP^{+}$ cells was counted per image, with $Axin2^{+}$ being defined as >20% above background levels.

For the IHC in Supplementary Fig. 1, coronal sections (50 μm thick) were made with a vibratome; sections were collected into antifreeze solution consisting of ethylene glycol, glycerol and PBS. Free-floating sections were blocked using 3% BSA in 0.1% PBST for 1 h. The sections were stained for 48 h at room temperature with primary antibody, and overnight with secondary antibody. The sections were mounted with Prolong Antifade reagent with DAPI (Life Technologies). *Z*-stacked images were acquired with a Zeiss LSM780 multi photon confocal system and processed using ImageJ. The number of GFP^{+} cells containing β-catenin staining was quantified by requiring the presence of β-catenin in the nucleus. To quantify β-catenin protein expression, we used the rabbit-conjugated primary antibody for total β-catenin (9562; Cell Signaling). We also amplified GFP staining using a chicken-conjugated primary antibody for GFP (Aves Laboratory). Stains were visualized using Chicken-Cy2 and Rabbit-Cy3 secondary antibodies (Jackson Immunolabs).

FACS. $D2^{+}$ and $D2^{-}$ cells from the NAc of D2-GFP mice were isolated using a fluorescence-assisted cell sorting (FACS) protocol. Briefly, 48 h after our standard CSDS protocol, bilateral 12 gauge punches were taken from the NAc and digested with an enzyme cocktail for 30 min at 37 °C before being triturated to obtain a homogeneous cellular preparation. Cells were then processed through a gradient, washed, and labelled with DAPI (viability marker) before being processed through an Influx sorter (BD Bioscience). $D2^{+}$ MSNs were sorted based on the size, internal complexity, and intensity of fluorescence with D2 cells emitting in the green channel (GFP). RNA was isolated using the Direct-zol RNA miniprep (Zymo Research) kit and cDNA was synthesized using the Iscript kit (Biorad). We confirmed the enrichment of D2 MSN-enriched genes in $D2^{+}$ cells and D1 MSN-enriched genes in $D2^{-}$ cells.

Quantitative chromatin immunoprecipitation (qChIP). Four 14 gauge NAc punches from each mouse were placed in 1% formaldehyde in 1× PBS to fix the DNA with the associated proteins. After 12 min on the rotator, 2 M glycine was added to stop the fixation for 5 min. The punches were then placed on ice and rinsed 5× with ice-cold PBS. Tissue from 5 animals were pooled at this point and homogenized in SDS lysis buffer (10% SDS, 1 M Tris-HCl, 0.5 M EDTA) with a desktop sonicator. ChIP dilution buffer (10% Triton X-100, 5 M NaCl, 1 M Tris-HCL pH 8.1, 0.5 M EDTA, 10% SDS and protease inhibitors) was added and the chromatin underwent high power sonication with the Bioruptor for 30 cycles of 30 s on/30 s off on high power. Conjugated magnetic beads were used to IP β-catenin with the ChIP-validated β-catenin antibody (Cell Signaling no. 4176) overnight in block solution (0.5% BSA in 1× PBS). The IP reaction was collected with a magnetic rack, washed, and both the input chromatin and the immunoprecipitated DNA were reverse cross-linked at 65° overnight. The DNA was then purified with RNase, proteinase K and the Qiagen PCR purification kit. The Qubit was used to quantify both the input and immunoprecipitated DNA and RT–PCR was used to quantify differential binding on the genomic DNA.

ChIP-seq. ChIP was performed for β-catenin as above. At the PCR purification step, however, 3 replicates were pooled onto one spin column so that each replicate became the pooled sample of 15 mice or 60 14 gauge NAc punches (4 NAc punches per animal), totalling ~100 mg wet weight tissue per library, following established protocols for brain. Animals were pooled so that social interaction times of different replicates across a group were approximately equal. ChIP-seq libraries were then prepared with the Illumina ChIP-seq kit as per their protocol. 2 replicates per condition were used for β-catenin while 3 replicates were used for histone mark experiments. Histone mark ChIP-seq was performed similarly except no further pooling was performed at the PCR purification step. Additionally, fragments from ~200–400 bp were size-selected for sequencing for β-catenin to compensate for the decreased yield of DNA. Libraries were validated on the Bioanalyzer for appropriate size selection and amplification before being sent to the Mount Sinai Genomics Core for sequencing. Homer[44] was used to identify peaks in individual conditions and NGS plot was used to create genome-wide overviews of binding at gene bodies[45]. We used hierarchical clustering based on the H3K4me3 data set to generate the heat map in Fig. 3c. To further validate our β-catenin data sets, we found that, in all 3 treatment conditions, IPA pathway analysis independently identified β-catenin as an upstream regulator due to the enrichment of known β-catenin target genes.

Small RNA-seq and analysis. Small RNA (<200 bp) was isolated and enriched with Qiagen RNeasy mini kit (catalogue no. 74104) following instructions. The small RNA was then used for library preparation following Epicentre Scriptminer small RNA library kit (catalogue no. SMSP10908) with optimization. In brief, a 3′ adaptor tag was ligated to the small RNA, then a 5′ adaptor oligonucleotide was attached following removal of excess 3′ adaptor oligonucleotide with degradase. The Di-tagged RNA was purified with Zymo RNA Clean & Concentrator Kits (catalogue no. R1015) and followed with reverse transcription into cDNA using the cDNA Synthesis Primer and MMLV Reverse Transcriptase. After removing RNA template by addition of RNase, the di-tagged cDNA was amplified and individually barcoded with nine PCR cycles using indices and PCR primers provided in the kit. The library was purified with Zymo DNA Clean & Concentrator kit (catalogue no. D4003) and size selected with Pippin (Sage Science). The library concentration was confirmed on Agilent Bioanalyzer before sequencing. Multiplexed libraries were then pooled and sequenced on an Illumina Hiseq sequencer. In total, 4–12 libraries/condition were included in this study. Raw sequencing reads were processed by cutadapt (https://code.google.com/p/cutadapt/) to remove adaptor sequence at 3′ end, and sequences shorter than 16 nucleotides after this were discarded. FastQC (http://www.bioinformatics.babraham.ac.uk/projects/fastqc/) was applied to inspect the sequencing quality. We ensured our small RNA sequencing was of good quality as the majority of reads aligned to mature miRNAs (Supplementary Table 3). miRanalyzer was used to align the short reads to genomic annotations and quantify the expression of the non-coding RNAs[46]. All miRNA annotations were downloaded from miRBase (v. 20)[47]. piRNA annotations were merged from piRNABank and NCBI[48,49]. tRNA and mRNA (RefSeq) annotations were downloaded from UCSC genome browser. The general ncRNA annotations were obtained from RFam (http://rfam.xfam.org/)[50]. The pipeline was organized by Ruffus (https://code.google.com/p/ruffus/), and the code is accessible from GitHub (https://github.com/shenlab-sinai/miRNA_pipeline_for_miRanalyzer)[51]. The differential expression detection was applied by DESeq2 (http://www.bioconductor.org/packages/release/bioc/html/DESeq2.html, http://biorxiv.org/content/early/2014/02/19/002832) with cut-offs of fold change 1.3 and P value < 0.05.

Statistics. One- or two-way analysis of variance (ANOVA) followed by Tukey's multiple comparison test, or two-way student's *t*-test were used for statistical analyses. All experiments represent at least 2–3 biological replicates unless otherwise indicated.

39. Robison, A. J. *et al.* Fluoxetine epigenetically alters the CaMKIIα promoter in nucleus accumbens to regulate ΔFosB binding and antidepressant effects. *Neuropsychopharmacology* **39,** 1178–1186 (2014).
40. Schmittgen, T. D. & Livak, K. J. Analyzing real-time PCR data by the comparative C_T method. *Nature Protocols* **3,** 1101–1108 (2008).
41. Lobo, M. K. *et al.* Cell type-specific loss of BDNF signaling mimics optogenetic control of cocaine reward. *Science* **330,** 385–390 (2010).
42. Koo, J. W. *et al.* BDNF is a negative modulator of morphine action. *Science* **338,** 124–128 (2012).
43. Chaudhury, D. *et al.* Rapid regulation of depression-related behaviours by control of midbrain dopamine neurons. *Nature* **493,** 532–536 (2013).
44. Heinz, S. *et al.* Simple combinations of lineage-determining transcription factors prime *cis*-regulatory elements required for macrophage and B cell identities. *Mol. Cell* **38,** 576–589 (2010).
45. Shen, L., Shao, N., Liu, X. & Nestler, E. ngs.plot: quick mining and visualization of next-generation sequencing data by integrating genomic databases. *BMC Genomics* **15,** 284 (2014).
46. Hackenberg, M., Rodríguez-Ezpeleta, N. & Aransay, A. M. MiRanalyzer: An update on the detection and analysis of microRNAs in high-throughput sequencing experiments. *Nucleic Acids Res.* **39** (Suppl. 2), W132–W138 (2011).
47. Griffiths-Jones, S. miRBase: the microRNA sequence database. *Methods Mol. Biol.* **342,** 129–138 (2006).
48. Sai Lakshmi, S. & Agrawal, S. piRNABank: a web resource on classified and clustered Piwi-interacting RNAs. *Nucleic Acids Res.* **36** (Suppl. 1), W173–W177 (2008).
49. Kozomara, A. & Griffiths-Jones, S. MiRBase: annotating high confidence microRNAs using deep sequencing data. *Nucleic Acids Res.* **42,** D68–D73 (2014).
50. Burge, S. W. *et al.* Rfam 11.0: 10 years of RNA families. *Nucleic Acids Res.* **41,** D226–D232 (2013).
51. Goodstadt, L. Ruffus: A lightweight python library for computational pipelines. *Bioinformatics* **26,** 2778–2779 (2010).

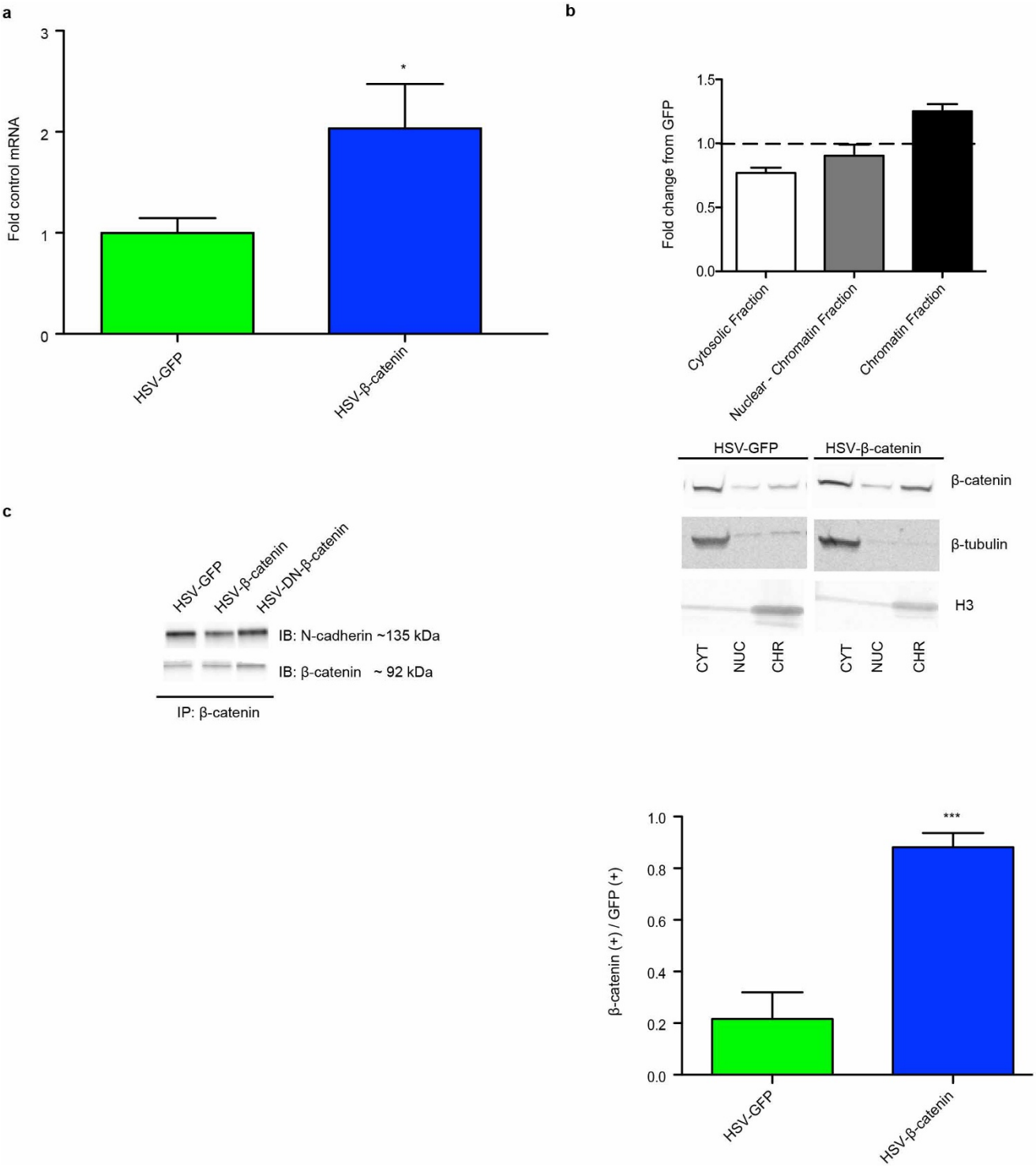

Extended Data Figure 1 | Validation of HSV-β-catenin. **a**, β-catenin mRNA levels following HSV-β-catenin versus HSV-GFP injection into NAc (*$P < 0.05$, two-tailed *t*-test, $n = 3$ per group). **b**, Top panel, subcellular fractionation of NAc lysates from HSV-GFP or HSV-β-catenin injected mice. Middle panel, representative western blots of data shown in panel **a**. CYT, cytosolic fraction; NUC, nuclear fraction (−chromatin); CHR, chromatin fraction. Bottom panel, IHC of nuclear β-catenin 5 days post-injection with HSV-β-catenin versus HSV-GFP (***$P < 0.001$, two-tailed *t*-test, $n = 3$ per group). **c**, β-catenin IP on virus-injected NAc. IP results are representative of 5 replications. All other data shown are representative of at least two experiments. Data are presented as mean and s.e.m.

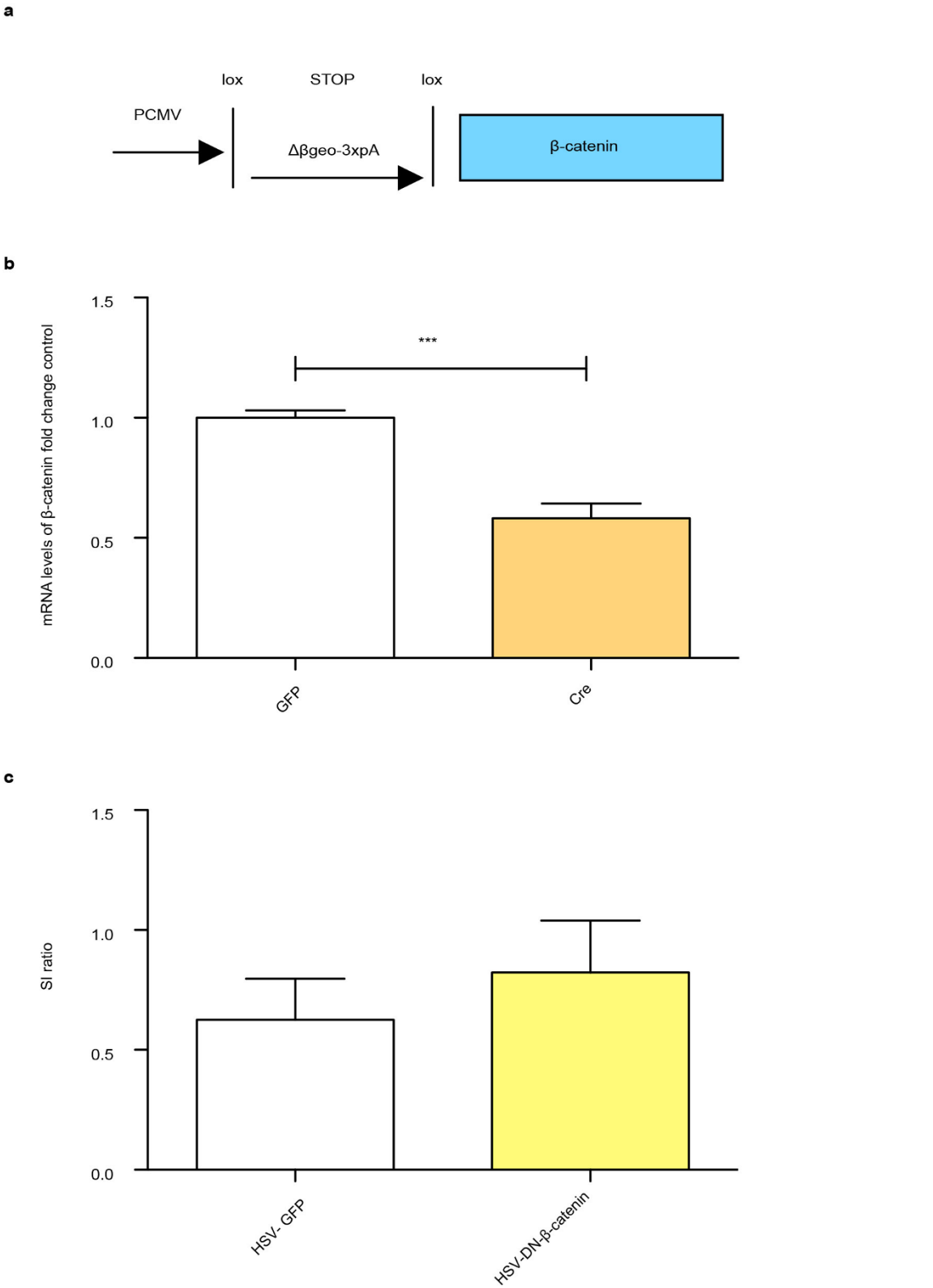

Extended Data Figure 2 | Other β-catenin manipulations. **a**, Schematic of Cre-dependent HSV-lox-stop (LS1L)-β-catenin cassette. **b**, Validation of β-catenin knockdown in the NAc of floxed β-catenin mice (***$P < 0.001$, two-tailed t-test, $n = 4$ GFP, $n = 5$ Cre). **c**, Failure of dominant negative β-catenin to rescue social interaction as compared to GFP after previous excision of β-catenin from NAc in floxed β-catenin mice undergoing defeat ($P > 0.05$, two-tailed t-test, $n = 7$ per group). Data are presented as mean and s.e.m. All data shown are representative of at least two experiments.

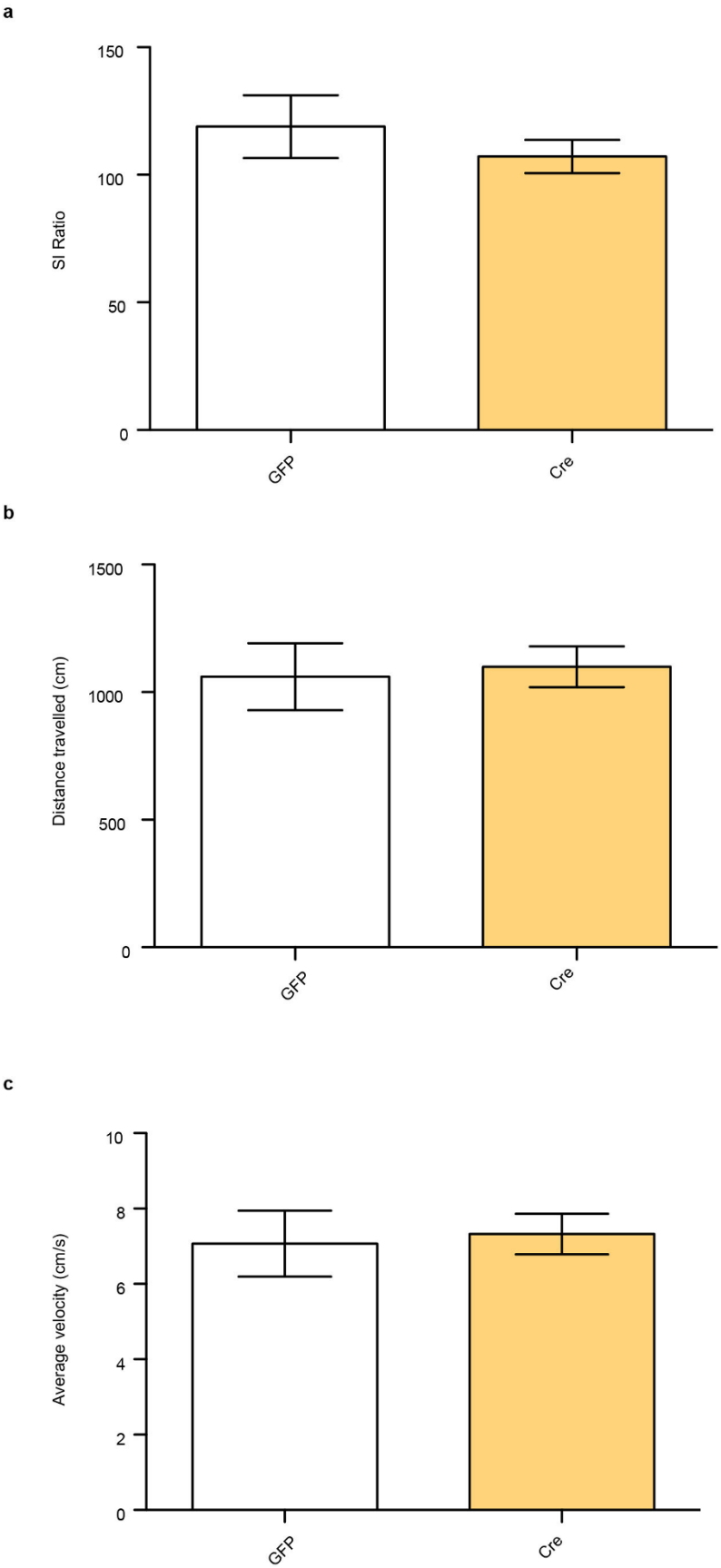

Extended Data Figure 3 | No effect of β-catenin deletion on baseline behaviours. **a**, Social interaction (SI) in control, non-stressed animals ($P > 0.05$, two-tailed t-test, $n = 5$ per group). **b**, Total distance travelled in arena ($P > 0.05$, two-tailed t-test, $n = 5$ per group). **c**, Average velocity ($P > 0.05$, two-tailed t-test, $n = 5$ per group). Data are presented as mean and s.e.m. All data shown are representative of at least two experiments.

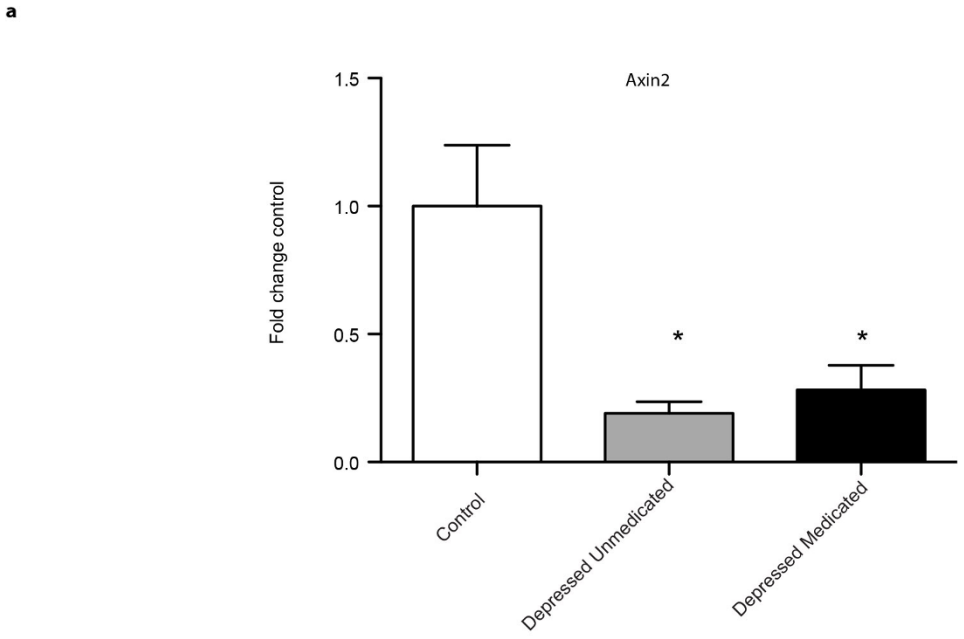

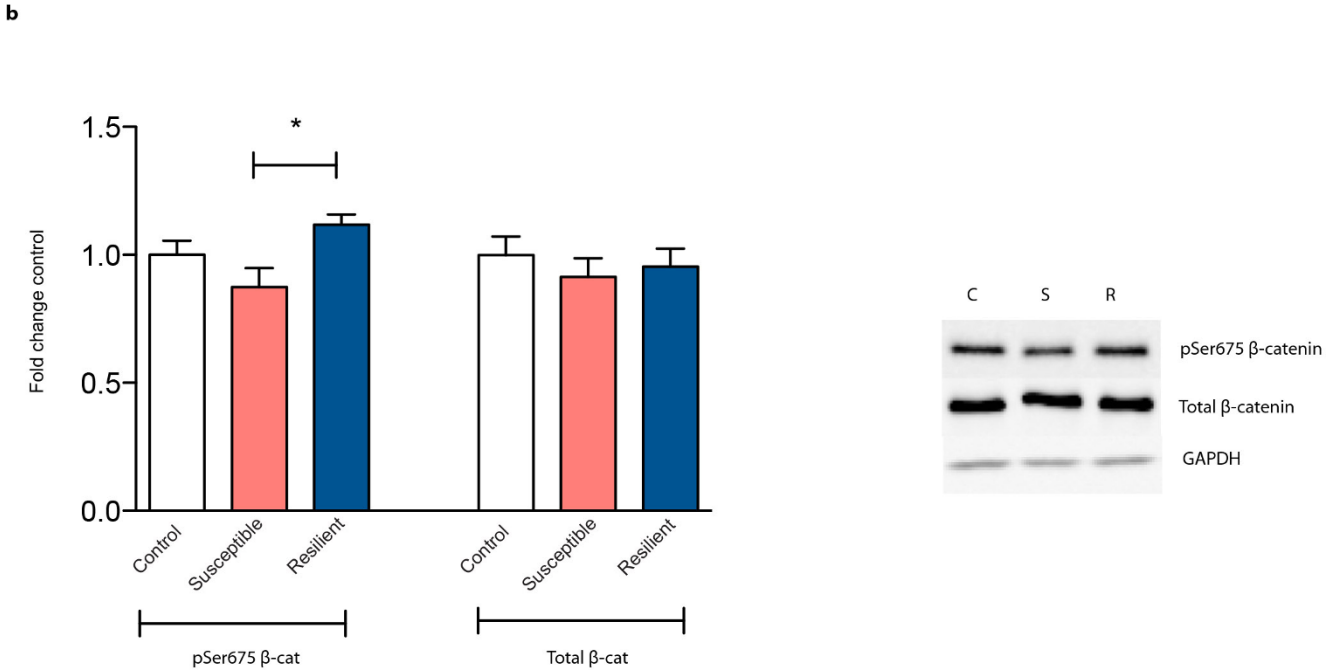

Extended Data Figure 4 | Regulation of β-catenin signalling in human depression and after CSDS in mice. a, Axin2 expression is suppressed in both medicated and unmedicated depressed patients, both groups of which were clinically depressed at their time of death ($P < 0.01$ one-way ANOVA, post-hoc test $P > 0.05$ between depressed unmedicated and medicated groups, $^*P < 0.01$ for either depressed group versus control, $n = 6$ control, $n = 5$ unmedicated depressed, medicated depressed). **b**, Phospho-Ser 675 β-catenin and total β-catenin levels from mouse control, susceptible, and resilient NAc 48 h post CSDS (phospho-Ser 675: $^*P < 0.05$, one-way ANOVA, post-hoc test susceptible versus resilient, $n = 5$ for control, susceptible, $n = 8$ for resilient). Data are presented as mean and s.e.m. Human data are from one experiment. All other data shown are representative of two experiments.

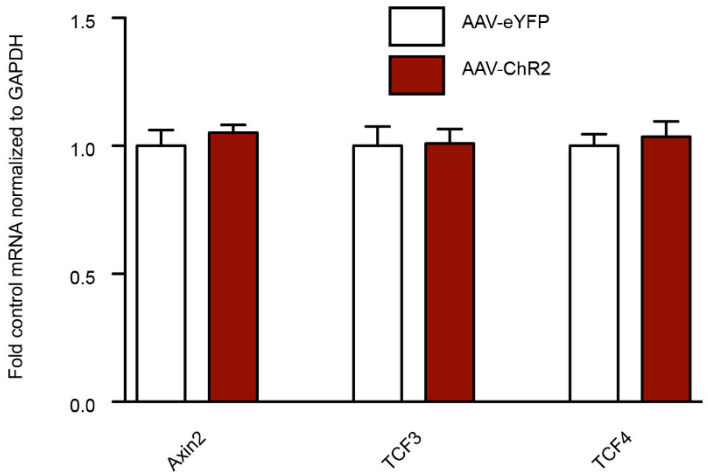

Extended Data Figure 5 | Repeated optogenetic burst stimulation of VTA cell bodies has no effect on canonical β-catenin signalling in NAc. Experiment was performed as in Fig. 2 with the exception of the optic fibre, which was placed above VTA for cell body stimulation ($P > 0.05$, two-tailed t-test, $n = 8$ per group). Data are presented as mean and s.e.m. Data are from one experiment.

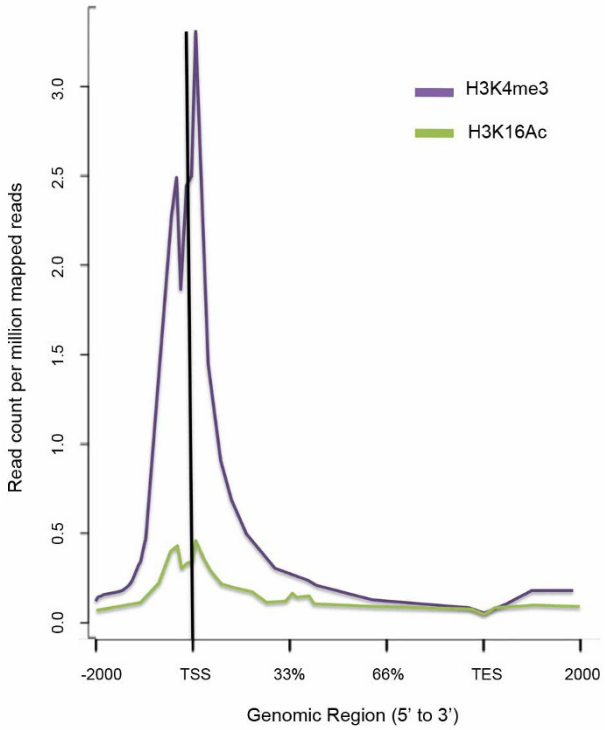

Extended Data Figure 6 | Genome-wide enrichment of H3K4me3 and H4K16ac binding in NAc at TSSs. NGS plot was used to visualize binding patterns.

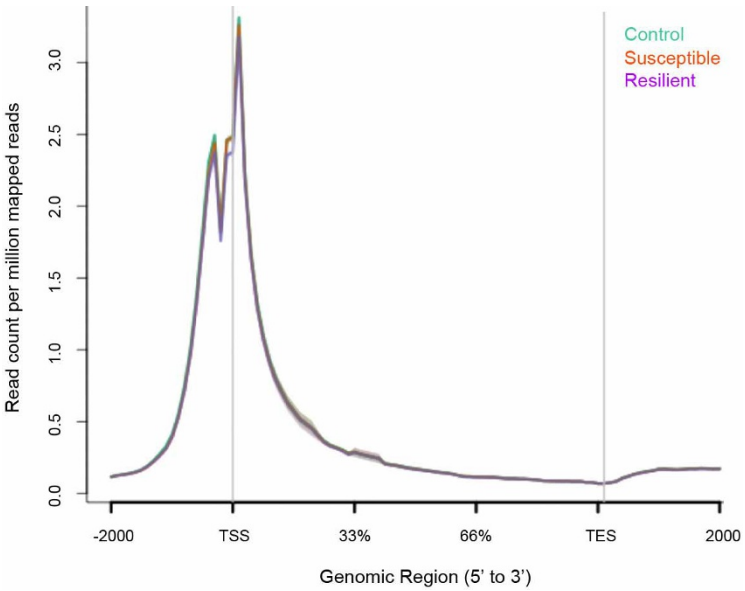

Extended Data Figure 7 | Genome-wide pattern of H3K4me3 binding to genic regions in NAc under control, susceptible (defeat), and resilient mice. Note the lack of difference across the three conditions. Data are from one experiment.

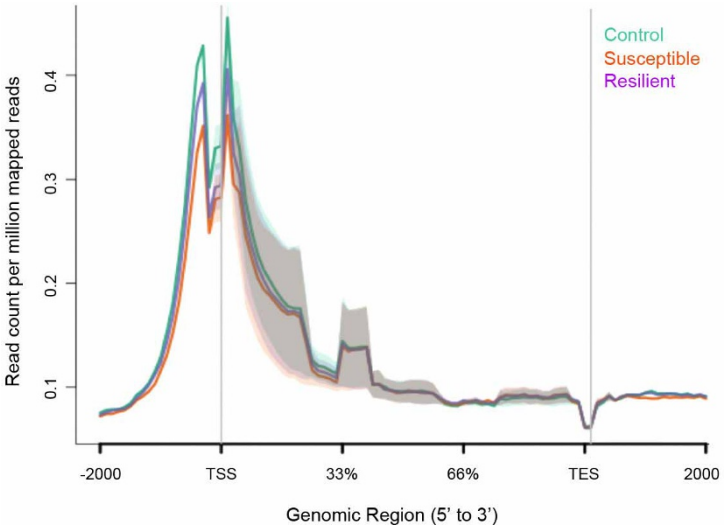

Extended Data Figure 8 | Genome-wide pattern of H4K16ac binding to genic regions in NAc under control, susceptible (defeat), and resilient mice. Note the lack of difference across the three conditions. Shading represents standard error. Data are from one experiment.

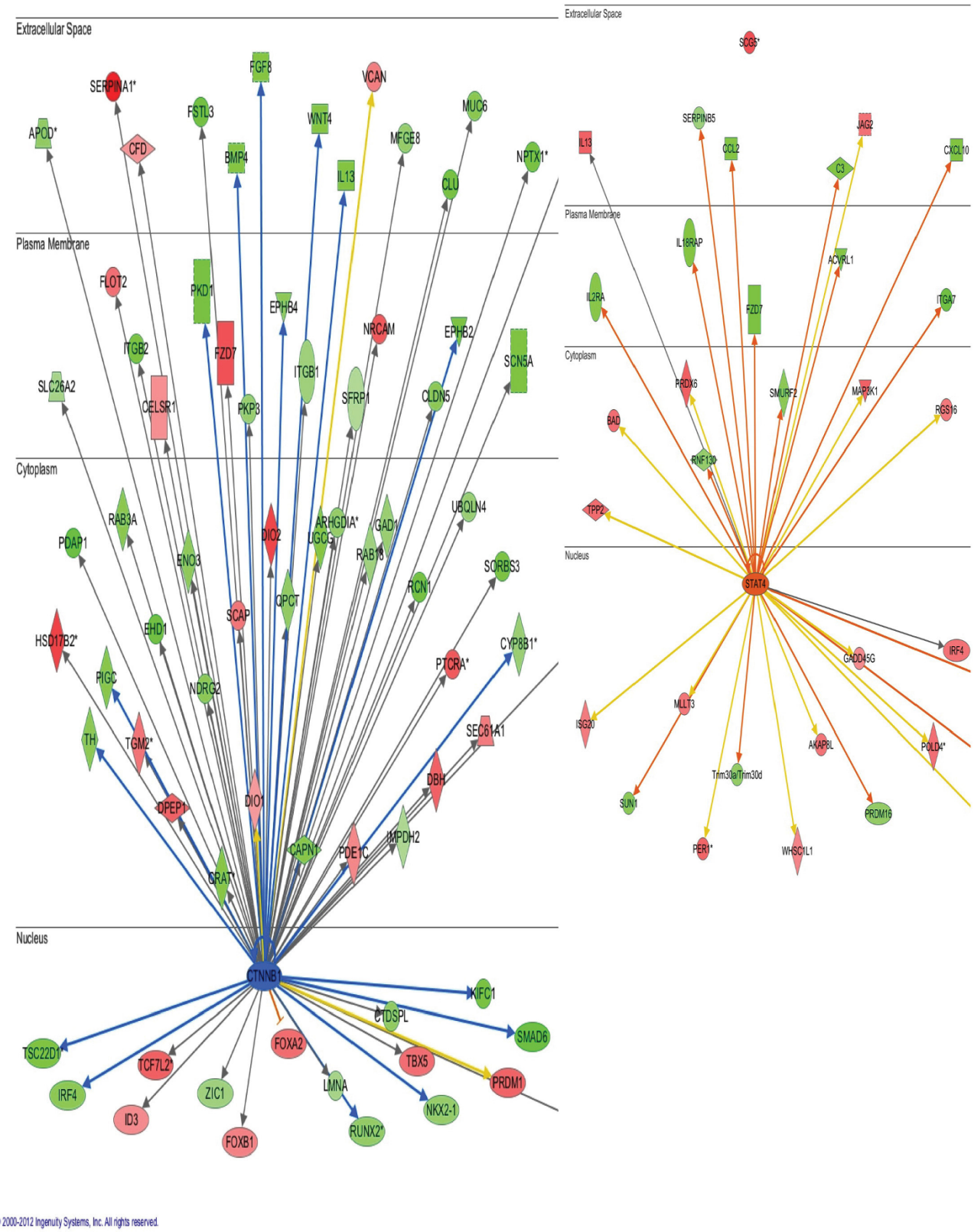

Extended Data Figure 9 | Ingenuity pathway analysis (IPA) identifies a network of genes that show upregulated β-catenin binding at promoter regions in the NAc of resilient versus susceptible mice. Nodes represent differentially regulated genes, with green meaning up in resilient versus susceptible and red meaning down in resilient versus susceptible. The blue arrows indicate that the direction of regulation is consistent with IPA prediction of an upregulated β-catenin network in resilience; for example, a blue arrow means that a target gene that would be expected to be upregulated by β-catenin is in fact upregulated in this list. In contrast, yellow arrows indicate that the regulation observed is inconsistent with expectations, while grey arrows indicate lack of pre-existing data to formulate expectations of β-catenin action. Left panel shows mostly expected regulation of the β-catenin network (that is, upregulation) in resilience; right panel shows non-specific changes occurring in a randomly chosen signal transducer and activator of transcription-4 (STAT4) network.

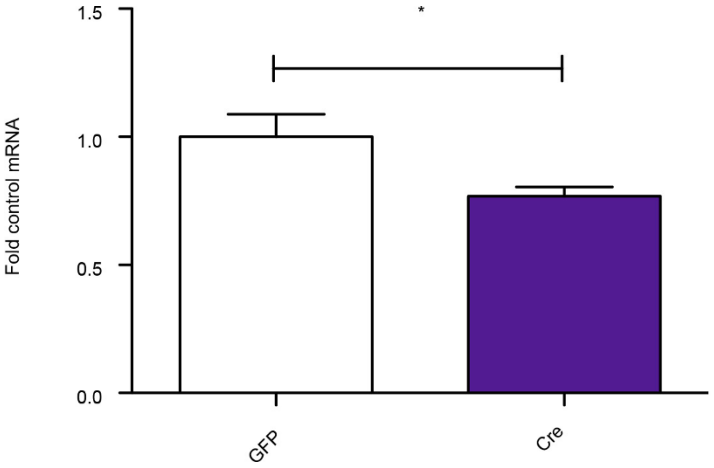

Extended Data Figure 10 | Validation of local Dicer1 knockdown. Note significant knockdown of Dicer expression in NAc after intra-NAc delivery of viral-Cre to floxed Dicer mice (*$P < 0.05$, two-tailed t-test, $n = 7$ GFP, $n = 6$ Cre). Data are presented as mean and s.e.m. and are representative of two experiments.